applied optics

High-power lasers for directed-energy applications

PHILLIP SPRANGLE, BAHMAN HAFIZI,* ANTONIO TING, AND RICHARD FISCHER

Plasma Physics Division, Naval Research Laboratory, Washington DC 20375, USA
**Corresponding author: bahman.hafizi@nrl.navy.mil*

Received 20 May 2015; revised 14 July 2015; accepted 15 August 2015; posted 18 August 2015 (Doc. ID 240144); published 16 September 2015

In this article, we review and discuss the research programs at the Naval Research Laboratory (NRL) on high-power lasers for directed-energy (DE) applications in the atmosphere. Physical processes affecting propagation include absorption/scattering, turbulence, and thermal blooming. The power levels needed for DE applications require combining a number of lasers. In atmospheric turbulence, there is a maximum intensity that can be placed on a target that is independent of the initial beam spot size and laser beam quality. By combining a number of kW-class fiber lasers, scientists at the NRL have successfully demonstrated high-power laser propagation in a turbulent atmosphere and wireless recharging. In the NRL experiments, four incoherently combined fiber lasers having a total power of 5 kW were propagated to a target 3.2 km away. These successful high-power experiments in a realistic atmosphere formed the basis of the Navy's Laser Weapon System. We compare the propagation characteristics of coherently and incoherently combined beams without adaptive optics. There is little difference in the energy on target between coherently and incoherently combined laser beams for multi-km propagation ranges and moderate to high levels of turbulence. Unlike incoherent combining, coherent combining places severe constraints on the individual lasers. These include the requirement of narrow power spectral linewidths in order to have long coherence times as well as polarization alignment of all the lasers. These requirements are extremely difficult for high-power lasers.

OCIS codes: (010.1300) Atmospheric propagation; (010.1330) Atmospheric turbulence; (140.6810) Thermal effects; (140.3295) Laser beam characterization; (140.3298) Laser beam combining.

http://dx.doi.org/10.1364/AO.54.00F201

1. INTRODUCTION

Advances in solid-state lasers, i.e., slab and fiber lasers, have made them candidates for directed-energy applications [1–3]. To achieve the power levels needed for these applications, it is necessary to combine a large number of lasers and propagate the beam many kilometers through a turbulent atmosphere.

In 2005, scientists at the Naval Research Laboratory (NRL) proposed, analyzed, and simulated the use of incoherently combined, high-power fiber lasers for directed-energy (DE) applications [4–8]. The patented NRL laser beam-combining architecture [9] is considered a promising approach for developing tactical laser weapons and forms the basis for the Navy's Laser Weapon System (LaWS) [10]. Shortly after the initial analysis and simulation of the concept, NRL scientists and team members from the Naval Surface Warfare Center carried out the first long-range field experiments. These laser beam combining and propagation experiments provided critical basic information addressing the issues associated with incoherently combined, high-power, single-mode fiber lasers.

In this NRL review article, we discuss the physical processes associated with the propagation of high-power lasers. Specifically, we discuss the effects of absorption/scattering, turbulence, and thermal blooming. We compare the energy delivered to a target for the case of coherently combined and incoherently combined laser beams. It is pointed out that for multi-km ranges and moderate to high levels of turbulence there is little difference in the energy delivered to the target. Coherent combining places severe constraints on the individual lasers. These include the requirement of narrow power spectral linewidths in order to have long coherence times, as well as polarization alignment of all the lasers. These requirements are extremely difficult for high-power lasers. Incoherently combined architecture, one the other hand, is far simpler to implement. Individually controlled steering mirrors with adaptive optics capabilities form the beam director and direct each beam to the target, as indicated schematically in Fig. 1. This beam-combining architecture has the capability of employing adaptive optics to extend the range. To limit diffractive spreading of the laser beams over the range, the individual spot sizes (radius)

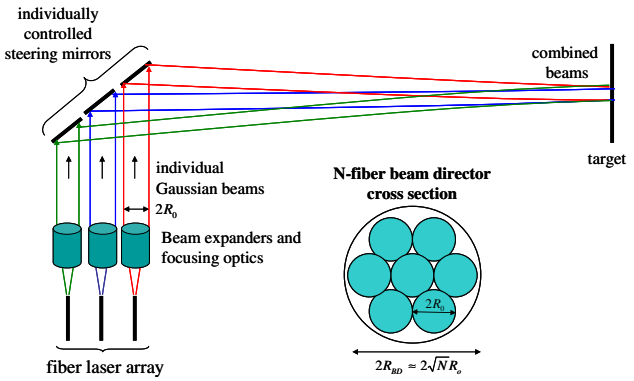

Fig. 1. Schematic diagram of incoherently combined fiber lasers individually directed to the target.

of the beams must be large enough at the source and have good optical quality.

Two experimental demonstrations of DE performed by NRL are reviewed and discussed: laser propagation in a turbulent atmosphere and wireless recharging.

2. ATMOSPHERIC PROPAGATION OF LASER BEAMS

A. Absorption/Scattering

Atmospheric propagation of laser beams is affected by the presence of molecules, atoms, and aerosols which scatter, as well as absorb, the laser energy [11,12]. Aerosols consist of soot, dust, and pollutants and in a maritime environment brine (salt water) can be the principal constituent. An approximate method for incorporating scattering and absorption of radiation is to introduce an extinction coefficient γ that takes into account the change in the intensity along the path z due to both absorption, α, and scattering, β, i.e., $\gamma = \alpha + \beta$. The laser intensity decreases exponentially according to $I(z) = I_0 \exp(-\gamma z)$, where I_0 is the initial laser intensity. The absorption (and scattering) of a laser beam can be small, e.g., $\alpha_M \approx 2 \times 10^{-10}$ cm^{-1}, $\beta_M \approx 10^{-8}$ cm^{-1} at a wavelength of 1.045 μm. Here, the subscript "M" indicates that the coefficient is due to the molecules. At the same wavelength, the aerosol absorption and scattering coefficients (subscript A) are much larger: $\alpha_A \approx 10^{-8}$ cm^{-1}, $\beta_A \approx 10^{-6}$ cm^{-1}. The effect of aerosols on laser beam propagation is significant because they scatter (and absorb) radiation collectively.

While both scattering and absorption reduce the on-axis intensity of the laser beam, at high powers absorption has the added effect of heating the medium along the path and causing thermal blooming. To minimize thermal blooming, it is necessary to reduce both the molecular absorption of the medium and the absorption due to aerosols. For thermal blooming to be manageable it is necessary to ensure that the aerosol absorption is small, which can be achieved by clearing the path by vaporizing the aerosols. In view of the strong dependence of α_A and β_A on the radius, vaporization can significantly reduce both the absorption and scattering.

B. Beam Spreading and Wander due to Turbulence

The refractive index is $n = 1 + \delta n_{Turb}(x, y, z, t)$, where the fluctuations δn_{Turb} satisfy $\langle \delta n_{Turb} \rangle = 0$ and $\langle \delta n_{Turb}^2 \rangle \neq 0$ [13–16]. The total angular spread of a laser beam can be written as $\Theta_{Spread} = (\Theta_{Diff}^2 + \Theta_Q^2 + \Theta_{Turb}^2 + \Theta_{Jitter}^2 + \Theta_{TB}^2)^{1/2}$, where the spreading angles are with respect to the propagation direction, Θ_{Diff} is due to diffraction, Θ_Q is due to the finite beam quality, Θ_{Turb} is due to turbulence, Θ_{Jitter} results from mechanical jitter, and Θ_{TB} is due to thermal blooming. For beams less than 100 kW, the contribution from thermal blooming can be generally neglected. The optical quality of a laser beam is measured in terms of the parameter M^2, which is referred to as "times diffraction limited." The angle $\Theta_{Diff} = \lambda/(\pi R_o)$ (Gaussian profile) is the angular spread of a diffraction-limited beam and $\Theta_Q = (M^2 - 1)\Theta_{Diff}$ is the angular spread due to higher-order modes. For single-mode lasers ($\Theta_Q \sim 0$) and long ranges, turbulence dominates diffractive beam spreading. For multimode lasers, on the other hand, turbulence contributes significantly less to beam spreading than does beam quality, i.e., $\Theta_Q > \Theta_{Turb} > \Theta_{Diff}$.

Turbulence leads to spreading of the laser beam spot size R_s and wandering of the laser beam centroid R_w. Figure 2 shows the laser beam spot (dotted circles) at several instants in time. Over a time scale that is long compared with that associated with wander, one obtains the broadened spot shown by the large circle in Fig. 2.

Strong (deep) turbulence is characterized by a Rytov number (log-amplitude variance) of $\sigma_\chi^2 > 0.25$. The Rytov variance (log-intensity) is given by $\sigma_R^2 = \exp(4\sigma_\chi^2) - 1$, which is approximately equal to $4\sigma_\chi^2$ for $\sigma_\chi^2 < 0.5$. Expressed in terms of the refractive index structure constant C_n^2, wavelength λ, and range L, the Rytov variance is $\sigma_R^2 \approx 4\sigma_\chi^2 = 10.5 C_n^2 \lambda^{-7/6} L^{11/6}$. The structure parameter C_n^2 typically is in the range of 10^{-15} – 10^{-13} m$^{-2/3}$ [13–16].

The time average laser intensity at range L, assuming a Gaussian profile, is

$$I(r, z = L) = I_o \frac{R_o^2}{R^2(L)} \exp(-2r^2/R^2(L)),$$

where the time-averaged laser spot size $R(L)$ is given by

$$R^2(L) = (\lambda L/\pi R_o)^2 (M^4 + 2.9(R_o/r_o)^2) + \Theta_{Jitter}^2 L^2 + R_o^2 (1 - L/L_F)^2, \quad (1)$$

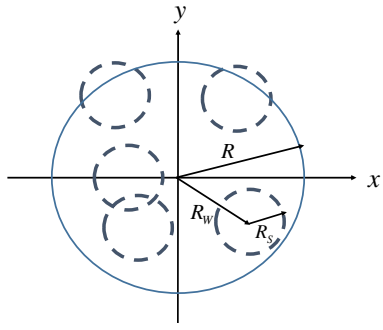

Fig. 2. Schematic showing the effects of turbulence. R_W is the centroid displacement (wander), and R_S is the increase in spot size (spreading), where $R \approx (R_W^2 + R_S^2)^{1/2}$.

where $R \approx (R_w^2 + R_s^2)^{1/2}$, R_o is the initial spot size, L_F is the focal length, and $r_o = 0.184(\lambda^2/C_n^2 L)^{3/5}$ is the transverse coherence length associated with turbulence. The beam centroid wander is given by $R_W^2 = 1.7(\lambda L/\pi R_o)^2 (R_o/r_o)^{5/3}$.

Adaptive optics can compensate for turbulence but not diffraction or poor beam quality. Therefore, while adaptive-optics techniques can enhance propagation efficiency for single-mode lasers, it would have little effect on multimode lasers. Some high-power lasers use a deformable mirror, camera, and feed loop to improve the beam quality of the transmitted beam. Tip–tilt correction is a type of adaptive optics that can be applied to the individual steering mirrors to minimize the overall combined laser spot size on target. Tip–tilt correction redirects the centroids of the individual laser beams to reduce the effects of wander due to turbulence. This is accomplished by monitoring the laser intensity on target and redirecting the individual steering mirrors. Laser beam centroid wander depends on the size of the turbulence eddies. Eddies that are large compared to the beam diameter cause the beam centroid to be deflected and wander in time due to lateral air flow. Small eddies, on the other hand, cause the beam's short-term spot size to spread about the centroid. The observed long-time averaged spot size is a combination of these two effects.

By appropriately modifying the wavefront of the transmitted beam, the laser power can be more effectively focused on target [14]. A beacon beam can be used to record the phase aberrations used to modify the amplitude and phase of the transmitted high-power beam. The information needed for modifying the amplitude and phase is obtained by phase-conjugating the beacon beam, i.e., $\exp(i\mathbf{k}\cdot\mathbf{r}) \rightarrow \exp(-i\mathbf{k}\cdot\mathbf{r})$. Phase conjugation can be achieved by using deformable mirrors or by a nonlinear optical mixing mechanism, e.g., four-wave Brillouin mixing [17–19]. Strong (deep) turbulence can have a significant, deleterious effect on the propagation of the HEL beam and conventional adaptive optics is ineffective.

C. Intensity Limit

The peak laser intensity on axis, at the target, is

$$I(r=0, z=L) = \left(\frac{6.28 P_T}{M^4 + 2.9(R_o/r_o)^2 + (\pi R_o \theta_{\text{jitter}}/\lambda)^2}\right)\left(\frac{R_o}{\lambda L}\right)^2 \exp(-\gamma L), \quad (2)$$

where P_T is the total transmitted laser power. When turbulence is sufficiently strong, i.e., $r_o < 1.7R_o/M^2$, the intensity on target reaches a maximum and Eq. (2) reduces to

$$I_{\max} = 2.17 P_T (r_o/\lambda L)^2 \exp(-\gamma L), \quad (3)$$

where mechanical jitter has been neglected. It is important to note that this maximum intensity is independent of the initial spot size and beam quality. Increasing the aperture size or improving beam quality will not increase the intensity on target. For typical parameters, this maximum intensity is obtained for modest initial laser spot sizes of $R_o \geq 10$ cm.

In Fig. 3, the laser intensity contours are shown for three levels of turbulence [20]. In limited or extremely weak turbulence [$C_n^2 = 0, \sigma_R^2 = 0$, Fig. 3(a)], the laser intensity is well defined with a relatively small spot size. In moderate turbulence [$C_n^2 = 10^{-14}$ m$^{-2/3}$, $\sigma_R^2 \approx 0.1$, Fig. 3(b)], the laser profile is distorted and the spot size is larger. In strong turbulence [$C_n^2 = 10^{-13}$ m$^{-2/3}$, $\sigma_R^2 \approx 1$, Fig. 3(c)], the laser profile is highly distorted. For sufficiently strong turbulence, a single discernible, high-intensity region in the cross-section may not be obtained.

D. Thermal Blooming

Thermal blooming becomes an issue for multi-km ranges and multi-hundreds of kW power levels. Propagation of a high-energy laser beam results in a small fraction of the laser energy being absorbed by both the molecular and aerosol constituents of air. The absorbed energy locally heats the air and leads to a decrease in the air density which modifies the refractive index, given by $\delta n_{\text{TB}} = (n_0 - 1)\delta\rho/\rho_0$, where ρ_0 and $\delta\rho$ are the ambient and perturbed airmass densities, respectively. The refractive index variation leads to a defocusing or spreading of the laser beam known as thermal blooming [19,21–25]. The effect of thermal blooming can be estimated by the magnitude of the phase advance/delay caused by a change in refractive index, i.e., $2\pi\delta n_{\text{TB}} L/\lambda$. For $|\delta n_{\text{TB}}| \ll \lambda/L$, distortion due to thermal blooming is small.

For an isobaric process, $\delta\rho = -(\rho_o/T_o)\delta T$, the perturbed refractive index due to thermal blooming air evolves according to

$$\left(\frac{\partial}{\partial t} + \mathbf{V}_W \cdot \nabla - \frac{\kappa}{c_p \rho_o}\nabla^2\right)\delta n_{\text{TB}} = -\alpha_{\text{Total}}(n_o - 1) I/(c_p T_o \rho_o),$$

where κ is the thermal conductivity, c_p is the specific heat at constant pressure, and $\mathbf{V}_W$ is the wind or slew velocity. The isobaric regime is valid for times greater than the hydrodynamic time R/C_s, where R is the laser spot size and C_s is the acoustic speed. The rate of change of laser energy density absorbed in air determines the degree of thermal blooming and is given by the total absorption coefficient α_{Total}. The aerosol contribution to the overall absorption coefficient can be much larger than that of molecular water vapor. For example, in the "water window" at wavelength 1.045 μm, $\alpha_{WV} = 3 \times 10^{-5}$ km^{-1}, while the effective aerosol contribution can be up to two orders of magnitude larger.

3. HIGH-POWER LASERS

Solid state lasers, in particular fiber lasers, are one of the main candidates for efficient and compact directed-energy systems.

A. Fiber Lasers

A number of companies manufacture high-power fiber lasers. In particular, IPG Photonics currently can provide the highest average powers, producing over 10 kW per fiber of high-quality optical radiation [1–3]. Multi-kW, single-mode fiber lasers typically have a beam quality parameter of $M^2 \approx 1$, which implies that they have near-minimum diffraction spreading.

To operate in a single mode, the core of the fiber must be sufficiently small. For example, the IPG single-mode 1 kW fiber lasers have a mode field diameter of ~15 μm. On the other hand, multimode IPG fibers operating at >30 kW per fiber have a core radius of ~200 μm and a beam quality of $M^2 \sim 13$. These higher-power fiber lasers with larger values of M^2 have a

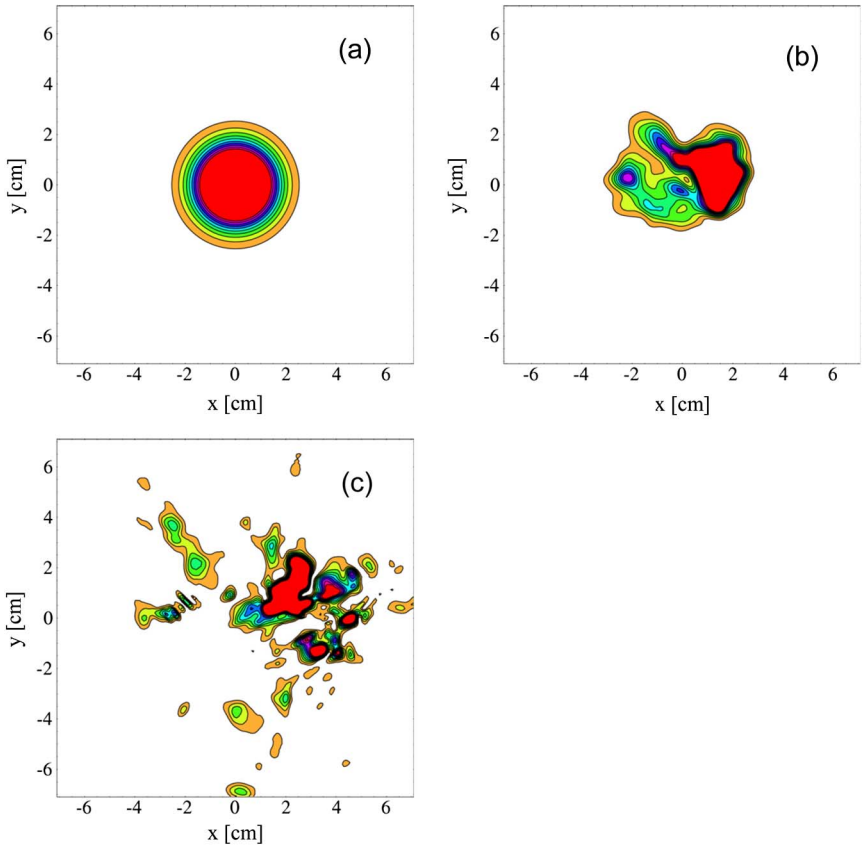

Fig. 3. Comparison of the intensity contours in the x-y plane at a range of 0.5 km for three levels of turbulence, (a) $C_n^2 = 0$, (b) $C_n^2 = 10^{-14}$ m$^{-2/3}$, and (c) $C_n^2 = 10^{-13}$ m$^{-2/3}$, using the NRL propagation code HELCAP [20].

more limited range (i.e., larger diffraction spreading angle). Multi-kW, single-mode fiber lasers have random polarization and large linewidth.

As an example, a 1 kW, single-mode IPG fiber laser module operating at 1.07 μm has a dimension of ~60 cm × 33 cm × 5 cm (excluding power supply), weighs ~20 lbs, and has an operating lifetime in excess of 10,000 h. Because of their high operating wall-plug efficiency (~30%) these lasers require only moderate cooling (i.e., ~2 gallons of water/minute/kW).

B. Beam Combining

To obtain the power levels necessary for DE applications, a large number of lasers must be combined. There are a number of approaches for combining the power from many lasers; they include spectral, coherent, and incoherent combining [8,26,27]. The following is a brief discussion and comparison of coherent and incoherent beam combining.

Coherent beam combining [27] relies on phase-matching the wavefronts of many lasers to produce high intensities on target [Fig. 4(a)]. The peak intensity on target is $N^2 I_o$, where I_o is the peak intensity of a single beam at the target and N is the number of combined beams. The diffraction length of the combined laser array is ~N times longer than that of the individual beams. However, as Eq. (3) indicates, even for relatively moderate turbulence, the peak intensity is essentially independent of aperture size so that the benefit of coherent combining

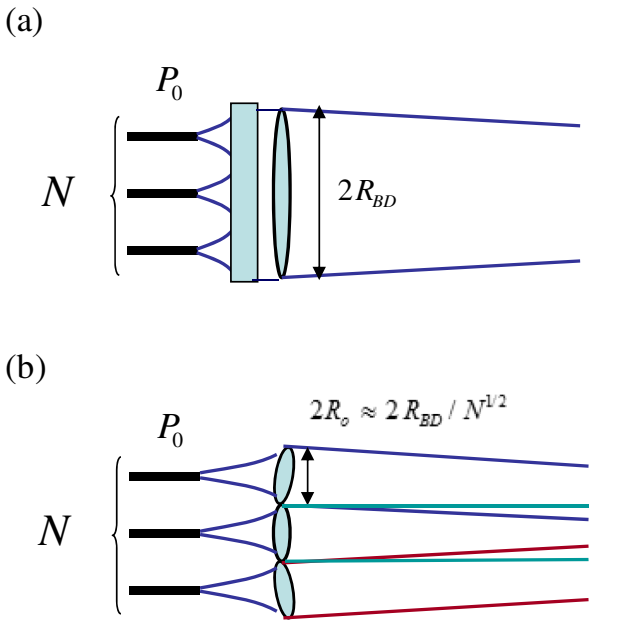

Fig. 4. Schematic of (a) coherently and (b) incoherently combined laser beams.

is lost. In addition, coherent combining can be difficult to achieve. It requires phase-locking and polarization-matching of the lasers, narrow linewidths ($\delta\lambda/\lambda < 10^{-6}$), and good optical beam quality. The propagation efficiency for coherent combining can also be limited by the filling factor of the laser array. A filling factor less than unity results in some of the laser energy residing in side lobes outside of the central lobe.

For incoherent combining [8], each beam is focused and directed to the target by individually controlled steering mirrors, Fig. 4(b). Incoherent beam combining does not require phase locking, polarization matching, or narrow linewidths. It should therefore result in a simpler and more robust system compared to the coherently combined configuration. The overall diffraction length is determined by the diffraction length of the individual beams. This is of little consequence for long-range propagation in moderate-to-strong turbulence since the intensity on target becomes independent of the initial spot size and beam quality [see Eq. (3)].

When comparing the two laser-combining architectures, we keep the size of the beam director and total transmitted power the same (Fig. 4). In order to minimize the number of parameters in the comparison, Gaussian beams are used in both beam-combining configurations. We assume that the laser linewidths are sufficiently small to be neglected. In both cases N beams are combined, either coherently or incoherently. A single Gaussian of initial spot size R_{BD} is used to model the N coherently combined beams [Fig. 4(a)] while for the incoherently combined beams [Fig. 4(b)], the initial spot sizes of the N beams are $\sim R_{BD}/N^{1/2}$. Although idealized models are used in the comparison, the conclusion is independent of whether the beams have a Gaussian, rectangular, or other profile. We find that for typical target ranges and levels of turbulence, the spot size on target is nearly the same for both beam-combining architectures [28].

To illustrate this point, consider the case where all beams in both architectures are focused on the target at range $L = L_F$. The spot size on target from Eq. (1) for the coherently combined and incoherently combined beams are, respectively, given by

$$R_{CC}(L) = (\lambda L/\pi R_{BD})(M^4 + 2.9(R_{BD}/r_o)^2)^{1/2}, \quad \textbf{(4a)}$$

$$R_{IC}(L) = (\lambda L/\pi R_{BD})(NM^4 + 2.9(R_{BD}/r_o)^2)^{1/2}, \quad \textbf{(4b)}$$

where mechanical jitter has been neglected and the beam quality associated with both configurations are taken to be the same and equal to M^2. In obtaining Eq. (4) from Eq. (1), the initial spot sizes for the coherently and incoherently combined beam configurations were taken to be $R_o = R_{BD}$ and $R_o \approx R_{BD}/N^{1/2}$, respectively. The only difference in Eqs. (4a) and (4b) is in the beam quality terms, i.e., terms proportional to M^4. The turbulence term dominates when the transverse coherence length satisfies the inequality

$$r_o < 1.7R_{BD}/(N^{1/2}M^2). \quad \textbf{(5)}$$

This condition is readily satisfied for moderate-to-strong levels of turbulence. As an example, for a laser wavelength of $\lambda = 1$ μm, moderate level of turbulence (i.e., $C_n^2 = 5 \times 10^{-14}$ m$^{-2/3}$), and range of $L = 2$ km, the transverse coherence length is $r_o \approx 1$ cm. The spot size on target is essentially the same for both beam-combining architectures [28].

In the absence of turbulence, perfect coherent combining has distinct advantages which include extended range and higher intensity on target. However, for long ranges, this advantage is reduced in typical levels of turbulence. For example, for typical horizontal propagation (i.e., $L \sim 5$ km range) and moderate levels of turbulence, the peak intensity and spot size on target are nearly identical for the two combining configurations. Hence, it is not necessary to have extremely high-quality beams, i.e., $M^2 < 3$ is sufficient. We also find that there is a maximum intensity on target which is independent of initial beam size and beam quality for km ranges and moderate turbulence.

There are a number of important issues to be considered before a coherent combining architecture can be used for DE applications. The following is a brief discussion of these issues.

To phase-lock lasers, the output phase information must be sent back to the input of the master oscillator which feeds the individual lasers. To be effective, the time scale required for this should be less than the laser coherence time $\tau_C = 1/\pi\Delta f$, where Δf is the power spectral frequency linewidth. The coherence time is the characteristic time over which the phase and intensity randomly vary, and is due solely to the finite spectral linewidth in the gain medium and the statistical nature of the emission from atoms or molecules.

Low-power experiments coherently combining seven fiber lasers were performed over a propagation range $L = 7$ km employing a target-in-the-loop feedback arrangement [29]. In these experiments, the total laser power was 12 mW, the transit time was $\tau_T = 2L/c = 50$ μs, and the coherence time was $\tau_C = 60$ μs ($\Delta f = 5$ kHz). Coherent combining was effective in these experiments only because at these low-power levels the linewidth of the lasers was very narrow, i.e., $\Delta\lambda/\lambda \sim 2 \times 10^{-11}$, and the level of atmospheric turbulence was low, i.e., $C_n^2 = 6 \times 10^{-16}$ m$^{-2/3}$, $r_o \approx 8$ cm, and $\sigma_R^2 \approx 0.7$.

High-power lasers, on the other hand, have significantly broader linewidths due to thermal Brillouin scattering, Doppler shift, self-phase modulation, and Raman broadening in the gain medium. For high-power lasers (multi-kW), the linewidth is typically $\Delta f = 1$ GHz and the coherence time is $\tau_C = 1/\pi\Delta f = 0.3$ ns [30] (for a Lorentzian spectral line shape). For these very short coherence times, corrections to the input phases will be extremely challenging.

In addition, high-power laser beams which have a finite power spectral linewidth will undergo phase mixing due to dispersion in air. Depending on the spectral line width, this effect could place additional limits on the ability to propagate coherently combined laser beams. A laser beam having a wavelength power spectral width of $\Delta\lambda$ will experience a phase spread given by $\Delta\theta = (\partial n/\partial\lambda)\Delta\lambda(2\pi/\lambda)L$ after propagating a distance L, which should be less than 2π. Here, $\partial n/\partial\lambda$ is the change in the refractive index of air with respect to wavelength. To maintain phase coherence to the target, the phase spread should be less than 2π. This condition translates into an inequality on the fractional power spectral linewidth of the laser beam, $\Delta\lambda/\lambda < (L\partial n/\partial\lambda)^{-1}$. As an example, for a wavelength

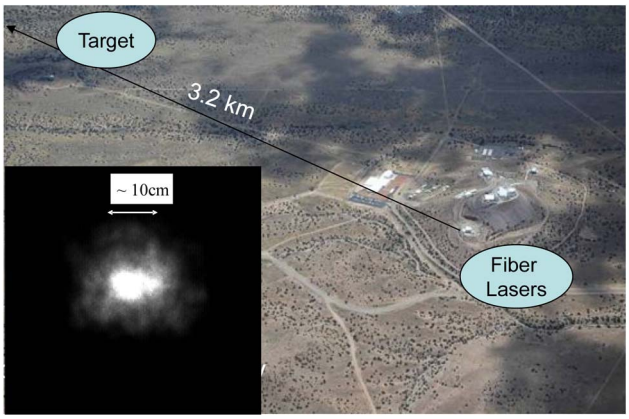

Fig. 5. NRL field experiments at the Star Fire Optical Range in New Mexico. In these experiments, four incoherently combined fiber lasers having a total power of 5 kW were propagated to a target 3.2 km away.

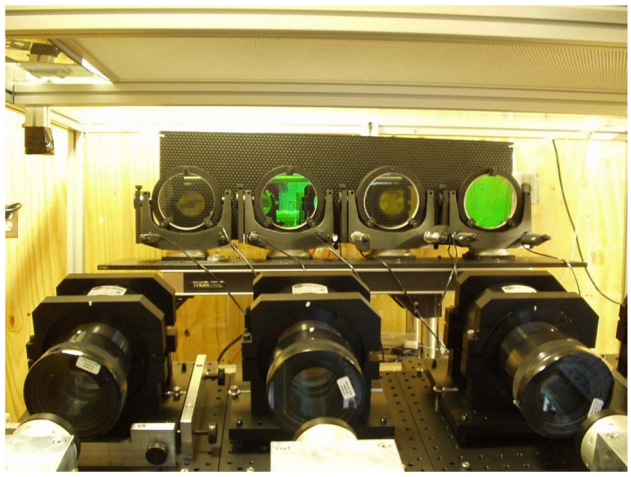

Fig. 6. NRL beam director used for incoherent combining. Three of four fiber laser collimators and beam expanders are shown in the foreground. Four individually controlled steering mirrors are shown in the background.

centered at $\lambda = 1$ μm, $\partial n/\partial\lambda = 3 \times 10^{-6}$ μm^{-1} for air. For a propagation distance of $L = 5$ km, the fractional linewidth should be $\Delta\lambda/\lambda < 7 \times 10^{-5}$. This condition on the fractional power linewidth may be difficult to achieve in high-power, multi-kW lasers.

In contrast to the low-power, coherent combining experiments in [29], NRL scientists in 2008–2009 performed field experiments at the Naval Surface Warfare Center in Dahlgren, Virginia and the Starfire Optical Range (SOR) in New Mexico. In the SOR experiments, four incoherently combined fiber lasers having a total power of 5 kW were propagated to a target 3.2 km away (Fig. 5). In these high-power incoherent combining experiments, the laser spot size (radius) on target was ~10 cm, the laser linewidth was $\Delta\lambda/\lambda \sim 5 \times 10^{-3}$, and the level of atmospheric turbulence was typically $C_n^2 = 10^{-14}$ m$^{-2/3}$, $r_o \sim 2.3$ cm, and $\sigma_R^2 \sim 2.8$. These successful high-power experiments in a realistic atmosphere formed the basis of the Navy's LaWS.

4. NRL LASER PROPAGATION AND WIRELESS RECHARGING EXPERIMENTS

A. Propagation in Turbulence

In this section, we discuss NRL scientists' role in developing the concepts that form the basis of the Navy's LaWS. Some of the objectives of the experiments were to validate the laser propagation models and to demonstrate the incoherent beam combining concept at long range and characterize laser beam wander and spreading.

The field experiments combined four single-mode fiber lasers using a beam director consisting of individually controlled steering mirrors [8]. Initial experiments took place at the Naval Surface Warfare Center in Dahlgren, Virginia, over a range of 1.2 km. The beam director consisted of four output couplers and four individually controlled steering mirrors as shown in Fig. 6. The laser spot size radius at the exit of the collimator was 1 cm and after the beam expander it was 2 cm. The radius of the water-cooled power meter (target) was 10 cm and the laser spot size on the target was 3 cm. These experiments demonstrated 90% propagation efficiency.

At high power, thermal expansion of optical elements (lenses, mirrors, etc.) becomes an important issue [31,32]. In these initial experiments, the fiber lasers were operated at nearly half power because of thermal effects in the beam director and in the atmosphere just beyond the laser source. These effects caused an axial shift of the focus with time, as the total laser power was increased. The change in the focal length was compensated for by changing the separation between the lenses in the beam expander. These thermal issues were corrected in the next series of experiments by using improved, low-absorption optics.

The experimental results were found to be in very good agreement with theory and simulations. Figure 7 shows simulation modeling of the laser intensity profiles at the beam director (panel a) and the combined beams at the target in simulation (panel b) and experiment (panel c). The next series of NRL field experiments was performed in 2008 at SOR at an increased range, and tip–tilt control of the incoherently combined laser beams was employed. Immediately following these successful experiments, a Naval Sea Systems Command lethality/propagation program was initiated at Dahlgren using six fiber lasers, each having a continuous power of 5 kW, in conjunction with a joint Pennsylvania State University/Naval Surface Warfare Center Crane Division propagation program using 10 and 5 kW fiber lasers.

LaWS employs six fiber lasers, incoherently combined into a single beam focused on the target. The simplicity of this approach enabled the Navy to advance LaWS rapidly and cheaply and enabled its deployment in the Persian Gulf for at-sea tests. Figure 8 shows the Navy's fiber laser beam director [10].

B. Wireless Recharging

In conjunction with the availability of high-quality, high-power lasers, advances in photovoltaic (PV) converter technologies allow high-power wireless recharging (power beaming) of

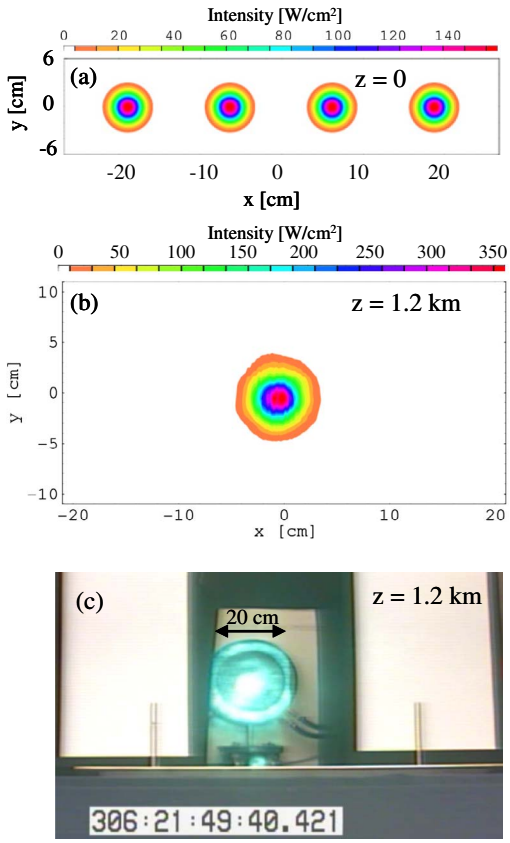

Fig. 7. Simulation showing a 2 s time-averaged transverse intensity profile of laser beams at (a) the source and (b) incoherently combined on target at a range of 1.2 km for a turbulence strength of $C_n^2 = 5 \times 10^{-14}$ $m^{-2/3}$, wind speed of 2.5 m/s, aerosol scattering coefficient of 0.05 km^{-1}, and mechanical jitter of 1–2 μm. The individual initial spot size is ~2.5 cm and the combined spot size on target is ~3–4 cm. (c) CCD camera image of four beams incoherently combined on target (20 cm diameter power meter) at a range of 1.2 km. The total transmitted power was 3 kW and the propagation efficiency ~90% in the experiment.

Fig. 8. Navy's LaWS is an example of a high-power laser suitable for remote wireless recharging. Shown are the beam director and tracking mount for combining and directing high-power fiber lasers.

platforms and sensors at extended ranges. These remote platforms may include airborne, land-based, or submerged vehicles, satellites, and sensors at hazardous locations. In addition, commercially available PV converters have advanced to a point where high conversion efficiency from laser energy to electrical energy is now possible.

In the 1890s, Nikola Tesla performed some of the first experiments demonstrating wireless recharging, using high-frequency electromagnetic radiation. Microwaves have since been used in short-range wireless recharging experiments because of their high-power conversion efficiency. However, for long-range recharging, large transmission and receiving antennas are required due to the longer wavelengths associated with microwave radiation. Long-range recharging can only be achieved using the significantly shorter wavelengths associated with lasers beams. The use of laser beams can significantly reduce the size and weight of the transmitting and receiving platforms.

Research groups at the National Aeronautics and Space Administration, Kinki University (Japan), LaserMotive Inc., and NRL have performed wireless recharging experiments on a variety of platforms such as rovers, kite planes, helicopters, and climbers using solid-state laser diodes and PV converters.

Figure 9 depicts a conceptual configuration for remote, wireless recharging of an unmanned aerial vehicle (UAV) using a high-power fiber laser and beam director. Turbulence and aerosols affect the propagation and delivery of the laser power to the platform.

Most PV cells are designed and developed for the conversion of the broad spectrum of solar energy into electrical power. The PV cell delivers the maximum optical-to-electrical conversion efficiency when illuminated by monochromatic (laser) light at a wavelength that closely corresponds to the bandgap energy of the PV material. Efficient PV cells based on Indium Gallium Arsenide (InGaAs) are now available commercially for laser wavelengths around 1 μm. An optimized PV converter on a remote platform, such as a UAV, can efficiently (50%–60%) convert laser energy to electrical power. A wireless recharging architecture using fiber lasers and PV cells can provide a significant weight reduction by removal of batteries, extended flight duration day and night, and extended range.

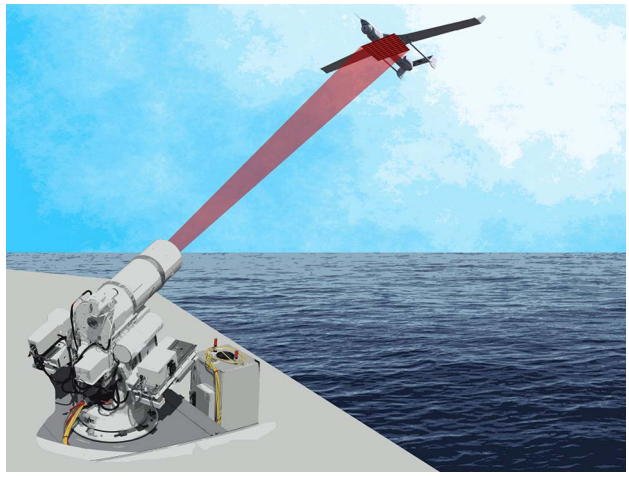

Fig. 9. Schematic of high-power laser wireless recharging of a UAV using a high-power continuous wave (cw) fiber laser.

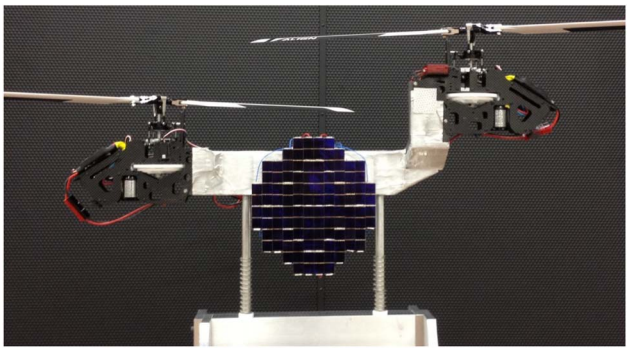

Fig. 10. Twin propeller aerial vehicle with a laser converter hanging in the middle. The PV cells convert laser power to electrical power at high efficiency and power the two propellers. The laser converter is cooled by the downdraft created by the propellers.

NRL demonstrated the recharging of a UAV in flight (at a range of 40 m) using a kilowatt-class fiber laser to transmit power and a PV cell for collection. Figure 10 shows a panel of highly efficient InGaAs PV cells on a laser converter panel. When illuminated with a high-power fiber laser, it converts the laser power to the electrical power required to power the twin propellers. The PV cells are connected in a configuration that matches the current and voltage characteristics required to drive the propellers. The laser converter has fins on its back to allow cooling by the downdraft of the propellers.

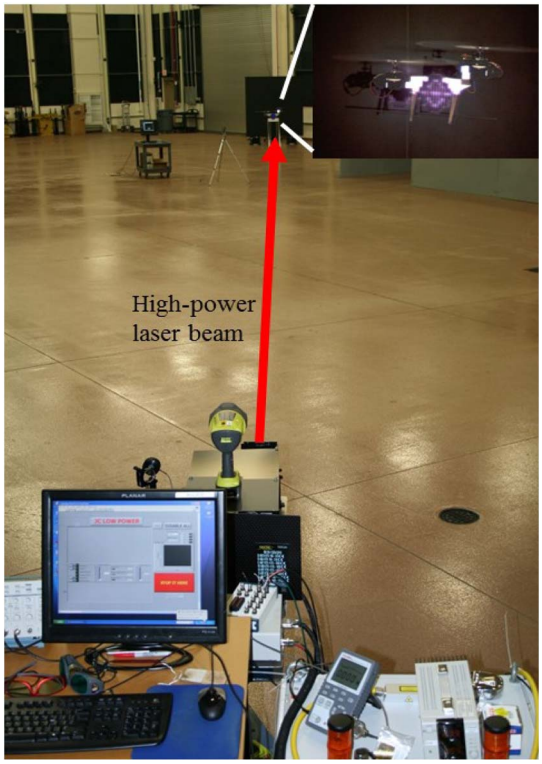

Fig. 11. Demonstration of laser recharging at a range of 40 m. The laser beam is shown by the red arrow propagating from the fiber laser collimator to the target, a twin propeller aerial vehicle with a laser converter in front. The vehicle under illumination is shown in the upper right inset where the converter appears violet and white. The high-power fiber laser can be seen in the lower right.

In 2013, a series of flight tests was successfully conducted over a 40-meter range at NRL's Laboratory for Autonomous Systems Research. In these tests, a high-power fiber laser was used to power a UAV. The experiment arrangement is shown in Fig. 11. A 2 kW, single-mode fiber laser (1.07 μm) transmits power to a PV array fabricated using InGaAs laser-power converter chips from Spectrolab Inc. The individual chips are 40%–50% efficient at the fiber laser wavelength, and the lightweight array provides 160–190 W of electricity to the vehicle. Off-the-shelf components were used to develop the optical tracking system, which automatically positioned the laser beam on the center of the laser converter during flight. In the experiment, the vehicle, remotely controlled, was able to lift off from rest on command. The aerial vehicle in flight under laser wireless recharging is shown in the inset in Fig. 11. The laser converter lights up in this image because the laser light, though in the infrared, is visible to the digital camera.

5. CHALLENGES

We have considered high-power laser propagation in turbulent atmosphere for two applications: DE weapons (LaWs) and wireless recharging. To fully realize the capabilities of LaWS for long-range (>5 km) and high, continuous power levels (more than 100 kW), issues such as adaptive optics for propagation in deep turbulence, thermal blooming, and thermal management in the director optics must be addressed. Similarly, there are a number of challenges to address before long-range wireless recharging can be deployed. These include the thermal management of the excess heat generated on the photovoltaic converter and development of higher-efficiency PV cells beyond 60% conversion. It is necessary to have a fairly uniform and controlled laser intensity profile on the photo-converter. This would require the development of appropriate adaptive optics techniques applied to the outgoing laser beam. For extended ranges, application of adaptive optics is necessary to control spreading and wander of the transmitted laser beam as it propagates through turbulence. Adaptive optics can be implemented by employing a beacon laser beam (low power) on the receiving platform to determine the phase variations placed on the beam due to turbulence. Introducing the conjugated phase variation on the high-power outgoing beam will minimize the effects of turbulence. Development of efficient, high-power lasers and PV converters operating in the eye-safe region (wavelengths of 1.5 μm and longer) may be necessary for certain applications. However, these challenges are of a technological nature and can be overcome in the near term.

In addition to UAVs, other unmanned systems also stand to benefit from wireless recharging. These include land-based vehicles and underwater vehicles. Atmospheric conditions for land-based vehicles, however, are quite different from those for UAV recharging. This is due to a high concentration of scattering particles affecting laser propagation. Underwater remote wireless recharging requires laser wavelengths in the blue–green regime.

Wireless recharging of low-flying satellites could also be viable to maintain their orbits. The atmospheric turbulence level

falls off extremely rapidly as a function of altitude. Hundreds of kilowatts of laser power can be delivered to the satellite at the perigee point (lowest height position, ~100 km) of the elliptical orbit. The laser intensity on the satellite PV cells can be several hundreds kW/m^2, which is hundreds of times the solar intensity (1 kW/m^2).

Funding. High-Energy Laser-Joint Technology Office; Naval Research Laboratory; Office of Naval Research (ONR).

REFERENCES

1. V. Gapontsev, "2 kW CW Yb-doped fiber laser with record diffraction limited brightness," in *The European Conference on Lasers and Electro-Optics (CLEO Europe)*, Munich, Germany, 2005, paper CJ1-1-THU.
2. J. Edgecumbe, D. Machewirth, J. Galipeau, B. Samson, K. Tankala, and M. O'Connor, "Kilowatt level, monolithic fiber amplifiers for beam combining applications at 1 μm," in *Proceedings of the 20th Solid State and Diode Laser Technology Review*, Los Angeles, California, 2007, paper FIB-2.
3. R. A. Motes and R. W. Berdine, *Introduction to High-Power Fiber Lasers* (Directed Energy Professional Society, 2009).
4. P. Sprangle, "Incoherent combining of high-power fiber lasers for long range DE applications," in *Proceedings of the 19th Solid State and Diode Laser Technology Review*, Albuquerque, New Mexico, 2006.
5. P. Sprangle, J. Peñano, A. Ting, and B. Hafizi, "Incoherent combining of high-power fiber lasers for long-range directed energy applications," NRL Memorandum Report, NRL/MR/6790–06-8963 (2006).
6. P. Sprangle, J. Peñano, B. Hafizi, and A. Ting, "Incoherent combining of high-power fiber lasers for long-range directed energy applications," J. Directed Energy **2**, 273–284 (2007).
7. P. Sprangle, J. Peñano, and B. Hafizi, "Optimum wavelength and power for efficient laser propagation in various atmospheric environments," J. Directed Energy **2**, 71–95 (2006).
8. P. Sprangle, A. Ting, J. Peñano, R. Fischer, and B. Hafizi, "Incoherent combining and atmospheric propagation of high-power fiber lasers for directed-energy applications," IEEE J. Quantum Electron. **45**, 1–2 (2009).
9. P. Sprangle, J. Peñano, B. Hafizi, A. Ting, and R. Fischer, "Apparatus for incoherent combining of high-power lasers for long-range directed-energy applications," U.S. patent 7970040 (28 June 2011).
10. P. Sprangle, B. Hafizi, and A. Ting, "NRL and the development of the laser weapon system," Future Force Nav. Sci. Technol. Mag. **2** (1), 18–21 (2015), winter.
11. P. Sprangle, J. Peñano, and B. Hafizi, "Optimum wavelength and power for efficient laser propagation in various atmospheric environments," NRL Memorandum Report, NRL/MR/6790-05-8907 (2005).
12. F. G. Smith, ed., *The Infrared and Electro-Optical Systems Handbook*, Vol. **2** of Atmospheric Propagation of Radiation (SPIE, 1993).
13. R. L. Fante, "Electromagnetic beam propagation in turbulent media," Proc. IEEE **63**, 1669–1692 (1975).
14. J. W. Hardy, *Adaptive Optics for Astronomical Telescopes* (Oxford University, 1998).
15. L. C. Andrews and R. L. Phillips, *Laser Beam Propagation through Random Media*, 2nd ed. (SPIE, 2005).
16. P. W. Milonni and J. H. Eberly, *Laser Physics* (Wiley, 2010).
17. A. E. Siegman, P. A. Belanger, and A. Hardy, "Optical resonators using phase conjugate mirrors," in *Optical Phase Conjugation*, R. A. Fisher, ed. (Academic, 1983).
18. M. D. Skeldon, P. Narum, and R. W. Boyd, "Non-frequency-shifted, high-fidelity phase conjugation with aberrated pump waves by Brillouin-enhanced four-wave mixing," Opt. Lett. **12**, 343–345 (1987).
19. R. W. Boyd, *Nonlinear Optics* (Elsevier, 2008).
20. J. R. Peñano, P. Sprangle, and B. Hafizi, "Propagation of high energy laser beams through atmospheric stagnation zones," J. Directed Energy **2**, 1–11 (2006).
21. F. G. Gebhardt and D. C. Smith, "Self-induced thermal distortion in the near field for a laser beam in a moving medium," IEEE J. Quantum Electron. **7**, 63–73 (1971).
22. D. C. Smith, "High power laser propagation: thermal blooming," Proc. IEEE **65**, 1679–1714 (1977).
23. J. A. Fleck, J. R. Morris, and M. D. Feit, "Time-dependent propagation of high energy laser beams through the atmosphere," Appl. Phys. **10**, 129–160 (1976).
24. J. A. Fleck, J. R. Morris, and M. D. Feit, "Time-dependent propagation of high energy laser beams through the atmosphere: II," Appl. Phys. **14**, 99–115 (1977).
25. B. Hafizi, J. Peñano, R. Fischer, G. DiComo, and A. Ting, "Determination of absorption coefficient based on laser beam thermal blooming in gas-filled tube," Appl. Opt. **53**, 5016–5023 (2014).
26. T. Y. Fan, "Laser beam combining for high-power, high-radiance sources," IEEE J. Sel. Top. Quantum Electron. **11**, 567–577 (2005).
27. A. Brignon, ed., *Coherent Laser Beam Combining* (Wiley-VCH, 2013).
28. P. Sprangle, J. Peñano, and B. Hafizi, "Beam combining and atmospheric propagation of high-power lasers," NRL Memorandum Report, NRL/MR/6790-11-9371 (2011).
29. T. Weyrauch, M. A. Vorontsov, G. W. Carhart, L. A. Beresnev, A. P. Rostov, E. E. Polnau, and J. J. Liu, "Experimental demonstration of coherent beam combining over a 7 km propagation path," Opt. Lett. **36**, 4455–4457 (2011).
30. D. Engin, W. Lu, M. Akbulut, B. McIntosh, H. Verdun, and S. Gupta, "1 kW cw Yb-fiber-amplifier with < 0.5 GHz linewidth and near-diffraction limited beam quality, for coherent application," Proc. SPIE **7914**, 791407 (2011).
31. J. Peñano, P. Sprangle, A. Ting, R. Fischer, B. Hafizi, and P. Serafim, "Optical quality of high-power lasers in lenses," J. Opt. Soc. Am. B **26**, 503–510 (2009).
32. B. Hafizi, A. Ting, D. Gordon, P. Sprangle, J. Peñano, R. Fischer, G. DiComo, and D. Colombant, "Laser heating of uncoated optics in a convective medium," Appl. Opt. **51**, 2573–2580 (2012).